THE CALIFORNIA-KEPLER SURVEY.

I. HIGH RESOLUTION SPECTROSCOPY OF 1305 STARS HOSTING KEPLER TRANSITING PLANETS¹

Erik A. Petigura^{2,11}, Andrew W. Howard^{2,3}, Geoffrey W. Marcy⁴, John Asher Johnson⁵, Howard Isaacson⁴, Phillip A. Cargile⁵, Leslie Hebb⁶, Benjamin J. Fulton^{3,2,12}, Lauren M. Weiss^{7,13}, Timothy D. Morton⁹, Joshua N. Winn⁹, Leslie A. Rogers¹⁰, Evan Sinukoff^{3,2,14}, Lea A. Hirsch⁴, Ian J. M. Crossfield^{8,15}

Submitted to AAS Journals

ABSTRACT

The California-Kepler Survey (CKS) is an observational program to improve our knowledge of the properties of stars found to host transiting planets by NASA's Kepler Mission. The improvement stems from new high-resolution optical spectra obtained using HIRES at the W. M. Keck Observatory. The CKS stellar sample comprises 1305 stars classified as Kepler Objects of Interest, hosting a total of 2075 transiting planets. The primary sample is magnitude-limited (Kp < 14.2) and contains 960 stars with 1385 planets. The sample was extended to include some fainter stars that host multiple planets, ultra short period planets, or habitable zone planets. The spectroscopic parameters were determined with two different codes, one based on template matching and the other on direct spectral synthesis using radiative transfer. We demonstrate a precision of 60 K in $T_{\rm eff}$, 0.10 dex in $\log g$, 0.04 dex in [Fe/H], and 1.0 km s⁻¹ in $V \sin i$. In this paper, we describe the CKS project and present a uniform catalog of spectroscopic parameters. Subsequent papers in this series present catalogs of derived stellar properties such as mass, radius and age; revised planet properties; and statistical explorations of the ensemble. CKS is the largest survey to determine the properties of Kepler stars using a uniform set of high-resolution, high signal-to-noise ratio spectra. The HIRES spectra are available to the community for independent analyses.

Subject headings: catalogs — stars: abundances — stars: fundamental parameters — stars: spectroscopic

1. INTRODUCTION

The NASA Kepler Mission (Borucki et al. 2010; Koch et al. 2010; Borucki 2016) has ushered in a new era in astronomy, in which extrasolar planets are known to be ubiquitous. The canon of Kepler papers contains descriptions of many remarkable planetary systems. The precision of Kepler photometry enabled the detection of planets as small as Mercury (Barclay et al. 2013),

¹ Based on observations obtained at the W. M. Keck Observatory, which is operated jointly by the University of California and the California Institute of Technology. Keck time was granted for this project by the University of California, and California Institute of Technology, the University of Hawaii, and NASA.

² California Institute of Technology, Pasadena, CA, 91125,

 3 Institute for Astronomy, University of Hawai'i at Mānoa, Honolulu, HI 96822, USA

⁴ Department of Astronomy, University of California, Berkelev, CA 94720, USA

⁵ Harvard-Smithsonian Center for Astrophysics, 60 Garden St, Cambridge, MA 02138, USA

⁶ Hobart and William Smith Colleges, Geneva, NY 14456, USA

⁷ Institut de Recherche sur les Exoplanètes, Université de Montréal, Montréal, QC, Canada

⁸ Astronomy and Astrophysics Department, University of Cal

⁸ Astronomy and Astrophysics Department, University of California, Santa Cruz, CA, USA

⁹ Department of Astrophysical Sciences, Peyton Hall, 4 Ivy Lane, Princeton, NJ 08540, USA

¹⁰ Department of Astronomy & Astrophysics, University of Chicago, 5640 South Ellis Avenue, Chicago, IL 60637, USA ¹¹ Hubble Fellow

¹² National Science Foundation Graduate Research Fellow

 13 Trottier Fellow

 $^{14}\,\mathrm{Natural}$ Sciences and Engineering Research Council of Canada Graduate Student Fellow

¹⁵ NASA Sagan Fellow

and the long, nearly uninterrupted dataset revealed a plethora of compact systems of multiple transiting planets (e.g. Kepler-11; Lissauer et al. 2011a). These iconic Kepler systems present opportunities to determine planet masses and orbital properties through dynamical effects (Ford et al. 2011; Lissauer et al. 2011b) and have inspired new classes of planet formation models (Hansen & Murray 2012; Chiang & Laughlin 2013). Circumbinary planets were found (Doyle et al. 2011), and searches for moons (Kipping et al. 2012) and rings (Heising et al. 2015) were attempted. Kepler also revealed planets resembling the Earth in size and incident stellar flux (Borucki et al. 2012, 2013; Quintana et al. 2014; Torres et al. 2015).

Doppler measurements of the masses of Kepler-discovered planets provided constraints on the composition of small planets extending down to the size of Earth (e.g., Kepler-78b; Howard et al. 2013; Pepe et al. 2013). Once the sample of such measurements was large enough, patterns began to emerge. Marcy et al. (2014) measured the masses of 49 planets and found evidence for a transition from rock- to gas-dominated compositions with increasing planet size (Weiss & Marcy 2014; Rogers 2015; Wolfgang & Lopez 2015).

The Kepler canon also includes statistical analyses of the properties of thousands of transiting planets and their host stars. Shortly before the launch of Kepler, radial-velocity (RV) surveys found that the occurrence of close-in (< 0.5 AU) planets around FGK stars rises rapidly with decreasing mass, with Neptune-mass planets outnumbering Jovian mass planets (Howard et al. 2010b; Mayor et al. 2011). After just a few months of Kepler photometry, the prevalence of planets smaller than Neptune ($R_P < 4.0 R_{\oplus}$) was confirmed and came into sharper

focus. Many studies quantified the occurrence of planets as a function of planet radius and orbital period (Howard et al. 2012; Petigura et al. 2013b; Fressin et al. 2013; Dressing & Charbonneau 2013). Further work showed that Earth-size planets are common in and near the habitable zone (Petigura et al. 2013a; Dressing & Charbonneau 2015; Burke et al. 2015).

A important limiting factor in large statistical analyses of *Kepler* planets is the quality of the host star properties. Using only broadband photometry, the Kepler Input Catalog (KIC; Brown et al. 2011) provided stellar effective temperatures and radii good to about 200 K and 30%. These parameters limit precision planet size and incident stellar flux measurements, obscuring important features. For example, any fine details in the radius distribution of planets are smeared out by the uncertainties associated with photometric stellar radii.

This paper introduces the California-Kepler Survey (CKS), a large observational campaign to measure the properties of *Kepler* planets and their host stars. CKS is designed in the same spirit as the pioneering spectroscopic surveys of nearby stars targeted in Doppler planet searches (Valenti & Fischer 2005). By providing a large sample of well-characterized stars, those early surveys mapped out the strong correlation between giant-planet occurrence and stellar metallicity (Fischer & Valenti 2005) and planet occurrence as a function of planet mass, stellar mass, and orbital distance (Cumming et al. 2008; Howard et al. 2010b; Johnson et al. 2010).

For the CKS project we measure stellar parameters and conduct statistical analyses of the Kepler planet population. A central motivation for CKS was to reduce the uncertainty in the sizes of Kepler stars and planets from typically 30% in the KIC to 10% using high-resolution spectroscopy. With this improvement, CKS enables more powerful and discriminating statistical studies of the occurrence of planets as a function of the properties of the planet and the host star, including its mass, age, and metallicity.

The CKS project grew out of experience with the Kepler Follow-up Observation Program (KFOP; Gautier et al. 2010), which carried out extensive ground-based observations of hundreds of Kepler Objects of Interest (KOIs) using many facilities operated by dozens of astronomers. These observations included direct imaging (Adams et al. 2012, 2013; Baranec et al. 2016; Ziegler et al. 2017; Furlan et al. 2017) as well as high-resolution spectroscopy (Gautier et al. 2012; Everett et al. 2013; Buchhave et al. 2012, 2014). The Spitzer Space Telescope was also used for characterization of Kepler-discovered planets (Désert et al. 2015).

In this paper, we describe the survey (Sec. 2), the spectroscopic pipelines (Sec. 3), the catalog of spectroscopic parameters (Sec. 4), a comparison of results from other surveys (Sec. 5), and a summary of conclusions (Sec. 6). Table 1 outlines the papers in the CKS series. Paper II presents the stellar radii, masses, and approximate ages for stars in the CKS sample, based on the spectroscopic parameters presented here. Papers III, IV, and V are statistical analyses of planet and star properties enabled

by this large and precise catalog. A set of related papers make use of the CKS data to conduct complementary analyses.

2. THE CALIFORNIA-KEPLER SURVEY

2.1. Project Plan

The original goal of the CKS project was to measure the stellar properties of all 997 host stars in the first large Kepler planet catalog (Borucki et al. 2011). As the Kepler planet catalogs grew in size (Batalha et al. 2013; Burke et al. 2014), we decided on a magnitude limit of Kp < 14.2 (Kepler apparent magnitude) for the primary CKS sample. Most of the spectra were collected during the 2012, 2013, and 2014 observing seasons. During this time the tabulated 'dispositions' of some KOIs changed between 'candidate', 'confirmed', 'validated', and 'false positive'. We discuss the dispositions that we adopted in Sec. 2.5. Planet candidates have low probabilities of being false positives, typically <10% (Morton & Johnson 2011). For simplicity, we refer to KOIs as "planets" throughout much of this paper, except when describing known false positives.

The CKS project is independent from the KFOP observations that were in direct support of the Kepler mission. CKS observations of the magnitude-limited sample (see Sec. 2.3) were conducted using Keck time granted for this project by the University of California, the California Institute of Technology, and the University of Hawaii. Observations of the sample of Multi-planet Systems were supported by Keck time from the University of California. The samples of Ultra-Short Period Planets and Habitable Zone Planets were observed using Keck time from NASA and the California Institute of Technology specifically for this project. Most of the CKS results $(\sim 1000 \text{ stars})$ are derived from spectra reported for the first time here. Some of the CKS stars ($\sim 300/1305$) were observed with Keck-HIRES as part of the NASA Keck time awarded to the KFOP team specifically for mission support and are included in CKS. Those previous observations were for characterization of noteworthy systems or as part of determining precise planet masses. The KFOP observations are described in Kepler Data Release 25 (DR25; Mathur et al. 2016) and include spectroscopic parameters that may vary slightly compared with our results. See Furlan et al., in prep. for a summary of KFOP spectroscopy. All spectra used in this paper are publicly available on Keck Observatory Archive.

2.2. Observations

We observed all 1305 stars in the CKS sample with the HIRES spectrometer (Vogt et al. 1994) at the W. M. Keck Observatory. We used an exposure meter to stop the exposures after achieving a signal-to-noise ratio (S/N) of 45 per pixel (90 per resolution element) at the peak of the blaze function in the spectral order containing 550 nm. A small subset of targets was observed at higher S/N, usually because a higher S/N was needed to serve as template spectra for precise RV measurements (Marcy et al. 2014). For the faintest targets (Kp > 15.0) the S/N was limited to \sim 20 per pixel, given the constraints on the total observing time. The spectral format and HIRES settings were identical to those used by the California Planet Search (Howard et al. 2010a). This includes the use of the B5/C2 decker with dimensions of

¹⁶ This effort was later enlarged to include any willing observers and renamed the Community Follow-up Observing Program (CFOP).

TABLE 1 PAPERS FROM THE CALIFORNIA KEPLER SURVEY

Primary CKS Papers

CKS I. High-Resolution Spectroscopy of 1305 Stars Hosting Kepler Transiting Planets (this paper)

CKS II. Precise Physical Properties of 2075 Kepler Planets and Their Host Stars (Johnson et al., submitted)

CKS III. A Gap in the Radius Distribution of Small Planets (Fulton et al., submitted)

CKS IV. Metallicities of *Kepler Planet Hosts* (Petigura et al., to be submitted) CKS V. Stellar and Planetary Properties of Kepler Multiplanet Systems (Weiss et al., to be submitted)

Related Papers Using CKS Data

Detection of Stars Within ${\sim}0.8^{\prime\prime} {\rm of}$ Kepler Objects of Interest (Kolbl et al. 2015)

Absence of a Metallicity Effect for Ultra-short-period Planets (Winn et al. 2017, submitted)

Identifying Young Kepler Planet Host Stars from Keck-HIRES Spectra of Lithium (Berger et al., in prep)

TABLE 2 CKS STELLAR SAMPLES

Sample	$N_{ m stars}$	$N_{ m planets}$
Magnitude-limited ($Kp < 14.2$)	960	1385
Multi-planet Systems	484	1254
Habitable Zone Systems	127	127
Ultra-Short Period Planets	71	71
Other	38	38
False Positives ^a	113	175
Total ^b	1305	2075

 $^{^{\}rm a}$ The False Positive sample includes systems for which all planet candidates have been dispositioned as false positives.

^b Some stars are in multiple samples.

 $0.86 \times 3.5 / 0.86 \times 14.0$, resulting in a spectral resolution of 60,000. For stars with V > 11 (most of the sample), we used the C2 decker and employed a sky-subtraction routine to reduce the impact of scattered moonlight and telluric emission lines (Batalha et al. 2011). The spectral coverage extended from 3640 to 7990 Å. We aligned the spectral format of HIRES such that the observatoryframe wavelengths were consistent to within one pixel from night to night. This allows for extraction of the spectral orders using the CPS raw reduction pipeline. We used the HIRES guide camera with a green filter (BG38), ensuring that the guiding signal was based on light near the middle of the wavelength range of the spectra. Except for a few stars with nearby companions, we used the HIRES image-rotator in the vertical-angle mode to capture the full spectral bandwidth within the spectrometer entrance slit.

$2.3.\ Stellar\ Samples$

The CKS sample comprises several overlapping subsamples listed below. Table 2 provides a summary of the number of stars and planets belonging to each subsample while Table 3 provides the star-by-star designations. Figure 1 shows the distribution of stellar brightness and of the number of planets per star, for the entire CKS sample.

 $\widehat{Magnitude}$ -limited. This sample is defined as all stars with Kp < 14.2. We set out to observe a magnitude-limited sample of KOIs chosen independent of the number of detected planets or previously measured stellar properties. As the project progressed, we added additional samples of fainter stars, as described below.

Multi-planet Systems. This sample is defined as KOIs stars orbited by two or more transiting planets (excluding

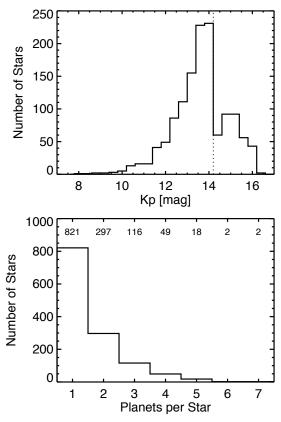


Fig. 1.— Properties of the CKS sample. Top: Distribution of stellar brightness in the Kepler bandpass (Kp). The dashed line at Kp=14.2 indicates that faint limit of the magnitude-limited sample. Bottom: Distribution of the number of planets per star. The label above each histogram bin specifies the number of stars belonging to that bin.

false positives). We also observed nearly all of the multi-transiting systems appearing in the Rowe et al. (2014) catalog, with priority given to the highest multiplicity systems and the brightest stars. CKS Paper V (Weiss et al. in prep.) performs a detailed analysis of the multiplanet systems.

Habitable-Zone Systems. We observed 127 host stars of Kepler planets residing in or near the habitable zone defined by (Kopparapu et al. 2013). Some of the individual habitable-zone planets have been studied extensively and validated (Borucki et al. 2013; Torres et al. 2015; Jenkins et al. 2015). It is not clear what to adopt as the boundaries of the liquid-water habitable zone, because of the

many uncertainties in exoplanet atmospheric properties and other factors that impact planet habitability (Seager 2013). The NASA Kepler Team constructed a list of habitable-zone targets using the best available stellar parameters at the time. They selected stars for which the flux received by the planet fell (within 1σ) between the Venus and "early-Mars" habitable-zone boundaries (Kopparapu et al. 2013). After the revision to the stellar parameters based on our CKS spectra, we now know that some of these planets are well outside of the habitable zone. CKS Paper II (Johnson et al., submitted) gives the newly determined values for stellar flux and planetary equilibrium temperature for all the CKS stars.

Ultra-Short Period Planets. Ultra-short period (USP) planets (Sanchis-Ojeda et al. 2014) have orbital periods shorter than one day. Winn et al. (2017, submitted) have performed an investigation of this sample, in particular on the metallicity distribution.

Other. We observed 38 additional Kepler planet host stars for reasons that do not fall into any of the preceding categories. Often these ad hoc observations were for studies of unusual or noteworthy planetary systems (e.g. Dawson et al. 2015; Désert et al. 2015; Holczer et al. 2015; Kruse & Agol 2014).

False Positives. The planetary candidate status ("disposition") of some KOIs has changed over time. Inevitably we observed KOIs that are now recognized as false positives. For completeness we report on the parameters for these false positives. Importantly, though, the false positives were not used for the cross-calibration between our two spectroscopic analysis pipelines (see Sec. 4.2). More details on this sample are given in Sec. 2.5.

It is important to recognize that the samples in the CKS survey are built upon the foundation of the Kepler mission. Assembling the Kepler planet catalogs required the extraordinary effort and devotion of the Kepler team members (Borucki et al. 2011; Batalha et al. 2013; Burke et al. 2014; Rowe et al. 2015). Also essential was the painstaking engineering behind the photometer (Caldwell et al. 2010; Gilliland et al. 2011; Bryson et al. 2010; Haas et al. 2010), as well as the software engineering that transformed CCD pixel values into planet candidates (Jenkins et al. 2010; Gilliland et al. 2010; Stumpe et al. 2012; Smith et al. 2012, 2016; Batalha et al. 2010a,b; Torres et al. 2011; Bryson et al. 2013; Christiansen et al. 2012, 2013, 2015, 2016; Thompson et al. 2015; McCauliff et al. 2015; Tenenbaum et al. 2013, 2014; Twicken et al. 2016; Kinemuchi et al. 2012).

2.4. Spectral Archive

All stellar spectra analyzed here are available to the public via the Keck Observatory Archive, ¹⁷ the Community Follow-up Program (CFOP) website, ¹⁸ and the CKS project website. ¹⁹ The CFOP website also contains additional information about each KOI and a discussion of the available follow-up observations. We have also made available the standard rest-frame wavelength solution applicable to every spectrum, which is accurate to within one pixel.

One auxiliary data product is the measurement of each star's velocity relative to the Solar System barycenter, as determined from measurements of the telluric absorption features (Chubak et al. 2012). These systemic radial velocities have a precision of $0.1 \, \mathrm{km \, s^{-1}}$ and are listed along with the spectroscopic parameters. Other auxiliary products are the stellar activity indicators that fall onto the HIRES format. The Ca II H & K measurements for this sample, in conjunction with stellar photometry, will be valuable when determining age-activity-rotation correlations (Isaacson & Fischer 2010). Figure 2 shows some typical CKS spectra containing the Mg I b region for a range of effective temperatures along the main sequence. In addition, Kolbl et al. (2015) consolidates all the available identifications of secondary spectral lines due to a second star that was admitted into the spectrometer slit.

2.5. False Positive Identification

"False positives" are KOIs that were initially classified as planet candidates, but later deemed to be non-planetary in nature. The most common types of false positives are foreground eclipsing binaries, background eclipsing binaries, and data artifacts. Statistical considerations of false positive scenarios suggest that false positives account for $\sim 10\%$ of all the planet candidates (Morton & Johnson 2011; Morton 2012; Fressin et al. 2013). KOIs hosting multiple planet candidates have an even lower false positive contamination rate of $\sim 1\%$ (Lissauer et al. 2012, 2014; Rowe et al. 2014). In contrast, Santerne et al. (2012) found a higher false positive contamination rate among gaint planet candidates of 30% through radial velocity follow-up.

False positives due to data artifacts can be caused by reflections from *Kepler*'s primary mirror and spillover light from eclipsing binaries that occupy nearby pixels on the *Kepler* CCD. Identifying false positives by matching KOI ephemerides to known eclipsing binaries revealed several hundred false positives and further improving the quality of later *Kepler* candidate lists (Coughlin et al. 2014).

We identified false positives in our sample by crossmatching with published false positive catalogs and online resources. In addition to planet catalogs produced by the Kepler team, detailed planet validation has been performed by Lissauer et al. (2012, 2014) on mulit-planet systems, and on large samples (1000's) of KOIs by Mullally et al. (2015) and Morton et al. (2016). The NASA Exoplanet Archive (Akeson et al. 2013) hosts a cumulative list of dispositions for every KOI. All of these catalogs combined provide high quality vetting of the Kepler planet candidate lists. Follow-up observations by the KFOP and community at large, using ground based facilities have also contributed heavily to false positive analysis as well as stellar classification, which has been used to improve the integrity of the planet candidate and confirmed planet lists.

For this work, we assign dispositions to the KOIs by referring to three catalogs. For each KOI, we first consult the catalog of Morton et al. (2016) and adopt that catalog's disposition whenever it is available. If the KOI does not appear in that catalog, we seek a disposition in the catalog of Mullally et al. (2015). If neither of those catalogs gives a disposition, we adopt the disposition of the NASA Exoplanet Archive. Our catalog does not con-

¹⁷ http://www2.keck.hawaii.edu/koa/public/koa.php

¹⁸ http://cfop.ipac.caltech.edu

¹⁹ http://astro.caltech.edu/~howard/cks/

-	$\Gamma ABLE$:	3
CKS	Target	Stars

			Stellar Sai	mples			
KOI No.	Magnitude-limited $(Kp < 14.2)$	Multi-planet Systems		Ultra-Short Period Planets	Other	All Planets are False Positives	
1	1	0	0	0	0	0	
2	1	0	0	0	0	0	
3	1	0	0	0	0	0	
6	1	0	0	0	0	1	
7	1	0	0	0	0	0	

Note. — This table will be published in its entirety in the machine-readable format in the accepted version of this paper. A portion is shown here for guidance regarding its form and content. Stars marked "1" are members of a stellar sample while those marked "0" are not.

 $\begin{array}{c} \text{TABLE 4} \\ \text{CKS Candidate Planets} \end{array}$

		False Positive Assessment						
KOI Candidate	Adopted Disposition ^a	Morton ^b	$Mullaly^c$	NEA^d				
K00001.01 K00002.01 K00003.01 K00006.01 K00007.01	CP CP CP FP CP	CP CP CP FP CP	CP CP CP FP CP	CP CP CP FP CP				

Note. — This table will be published in its entirety in the machine-readable format in the accepted version of this paper. A portion is shown here for guidance regarding its form and content.

tain any cases for which the KOI has conflicting dispositions of "false positive" and "confirmed-planet/planet-candidate". All the KOIs in our sample are either confirmed planets, planet candidates, or false positives. Table 4 gives the dispositions that follow from this procedure, and that are adopted for this and the subsequent CKS papers.

Upon closer examination of several KOIs for which our spectroscopic analysis produced suspect results, we identified 8 KOIs as false positives. Several are eclipsing binaries (KOIs 113, 134, 1032, 1463, 3419) and one is a brown dwarf (KOI-415) as determined with radial velocity measurements by Moutou et al. (2013). The transit signal detected in KOI-1546 was shown to arise from the variations of a different star in the field. KOI-1739 is a single-lined spectroscopic binary as determined via radial velocity measurements. The status of the latter two KOIs is documented on the CFOP. Because our spectroscopic pipelines assume a single spectrum, we removed the double-lined stars identified by Kolbl et al. (2015) from the CKS sample; the characteristics of those systems can be found in Table 9 of Kolbl et al. (2015).

3. SPECTROSCOPIC PIPELINES

We measured the stellar spectroscopic parameters using two independent data analysis pipelines: SpecMatch and SME@XSEDE. We describe these two pipelines in

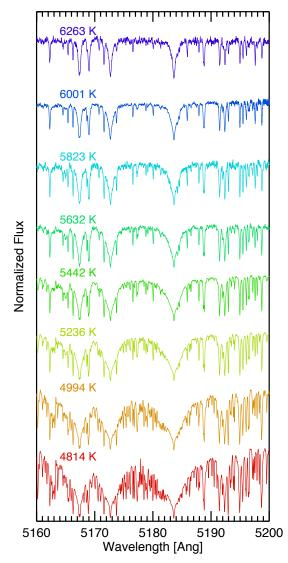


Fig. 2.— Keck-HIRES spectra spanning the Mg I b lines of eight slowly-rotating main sequence CKS stars, in ${\sim}200$ K increments of effective temperature.

Sec. 3.1 and 3.2, respectively. The two separate techniques permit the identification of suspect spectroscopic parameters by looking for large inconsistencies between the two methods. We describe the two analysis methods below. Sec. 4 gives the details of the construction of the

^a Dispositions: CP = confirmed planet; PC = planet candidate; FP = false positive.

^b Morton et al. (2016)

^c Mullally et al. (2015)

d NASA Exoplanet Archive, accessed 2017 February 1; http://exoplanetarchive.ipac.caltech.edu

combined catalog of stellar parameters.

3.1. SpecMatch

SpecMatch is a publicly-available²⁰

tool for precision stellar characterization, developed specifically for the CKS project, to accommodate spectra with a lower signal-to-noise ratio (S/N) than the usual spectra processed by the California Planet Search (CPS) team. Precision stellar characterization using HIRES spectra has been a key component in the exoplanet work of CPS for two decades. Typically, such analyses are performed using high signal-to-noise "template" observations, obtained during the course of the team's RV observations Marcy & Butler (1992). These template spectra typically have a S/N of 150-200 per HIRES pixel, permitting detailed modeling of several narrow regions of the spectrum with realistic stellar atmosphere models (Valenti & Fischer 2005). To compensate for the lower S/N of the CKS spectra, SpecMatch fits $\approx 400 \text{ Å}$ of the spectrum using computationally-efficient interpolation between precomputed model spectra, as opposed to detailed spectral synthesis.

Here, we offer a brief summary of the SpecMatch algorithm; for further details see Petigura (2015). SpecMatch fits five segments of an observed optical spectrum using forward-modeling. The code creates a synthetic spectrum of arbitrary $T_{\rm eff},$ $\log g,$ [Fe/H], and $V \sin i$ by first interpolating between model spectra computed by Coelho et al. (2005) at discrete values of T_{eff} , $\log g$, and [Fe/H]. Next, SpecMatch accounts for line broadening due to stellar rotation and convective macroturbulence by convolving the interpolated spectrum with the kernel specified by Hirano et al. (2011). Then, SpecMatch accounts for the instrumental profile of HIRES, which we model as a Gaussian having a FWHM of 3.8 HIRES pixels. We choose this value because it can reproduce the width of telluric lines observed through the "C2" decker for typical seeing conditions (see Petigura 2015 for further details). The version of SpecMatch used in this work has been slightly modified from the version presented in Petigura (2015). Instead of modeling all five spectral segments simultaneously, we model each segment individually and average the resulting parameters at the end. This modification improved run time, and the consistency of the parameters derived from individual segments provides a good check on the quality of the SpecMatch fits.

Petigura (2015) verified the precision and accuracy of SpecMatch parameters by comparisons with well-characterized touchstone stars from the literature. After calibrating the gravities to asteroseismic values computed by Huber et al. (2013), Petigura (2015) found that SpecMatch reproduces the surface gravities determined through asteroseismology to within 0.08 dex (RMS). Petigura (2015) demonstrated a precision in effective temperature and metallicity of 60 K and 0.04 dex, respectively, based on comparisons with Valenti & Fischer (2005). Finally, Petigura (2015) demonstrated a precision in projected stellar rotation, $V \sin i$, of 1.0 km s⁻¹, for $V \sin i \geq 2.0$ km s⁻¹.

Calibrating the SpecMatch $\log g$ values to the Huber et al. (2013) scale has the following shortcoming: the cal-

ibration is only valid over the domain of the HR-diagram containing stars with asteroseismic measurements, i.e. evolved stars and main sequence stars having spectral type \sim G2 and earlier. Extending the calibration toward later spectral types is a risky extrapolation, and reverting to the uncalibrated SpecMatch parameters introduces a discontinuous correction. Recently, Brewer et al. (2016) (B16 hereafter) extended the work of Valenti & Fischer (2005) by performing a detailed spectroscopic analysis of 1617 CPS target stars with updated version of SME (Brewer et al. 2015). The B16 catalog is an ideal calibration sample for SpecMatch because the spectroscopic surface gravities reproduce asteroseismic surface gravities to 0.05 dex and there is a large overlap in stars analyzed by both techniques.

We calibrated the SpecMatch parameters to the B16 scale by selecting 106 from the 1617 stars analyzed by B16 that spanned the following range of parameters: $T_{\rm eff} = 4700-6500$ K, $\log g = 2.50-4.75$ dex, and $[{\rm Fe/H}] = -1.0-+0.5$ dex. For each parameter, we derived a correction Δ that calibrates the SpecMatch parameters onto the B16 scale via ${\rm SM_{cal}} = {\rm SM_{raw}} + \Delta$. The corrections are linear (and therefore continuous) functions of the following form:

$$\begin{split} \Delta T_{\text{eff}} = & \, a_0 + a_1 \left(\frac{T_{\text{eff}} - 5500 \text{ K}}{100 \text{ K}} \right), \\ \Delta \log g = & \, b_0 + b_1 \left(\frac{\log g - 3.5 \text{ dex}}{0.1 \text{ dex}} \right) + b_2 \left(\frac{\text{[Fe/H]}}{0.1 \text{ dex}} \right), \\ \Delta [\text{Fe/H}] = & \, c_0 + c_1 \left(\frac{\text{[Fe/H]}}{0.1 \text{ dex}} \right), \end{split}$$

where $a_0=-61.9$ K and $a_1=6.13$; $b_0=-0.0234$ dex, $b_1=-0.0026$; and $b_2=-0.0412$, $c_0=0.0150$ dex, and $c_1=-0.0126$. The coefficients were chosen such that they minimized the RMS difference between the calibrated SpecMatch and B16 parameters (i.e. B16 – SM_{cal}). After applying these corrections, we compare the calibrated SpecMatch and B16 parameters in Figure 3. We find a dispersion of 61 K, 0.099 dex, and $0.06 \text{ dex in } T_{\text{eff}}, \log g, \text{ and } [\text{Fe/H}], \text{ respectively. By con-}$ struction, there is no mean offset between the calibrated SpecMatch and B16 parameters. We verified that the flexibility in our calibration was not misrepresenting the agreement between SpecMatch and B16 by comparing a distinct group of 80 stars that were not used in the calibration. The agreement between B16 and SpecMatch was comparable for this second set of stars: RMS dispersions were 55 K, 0.10 dex, and 0.05 dex for $T_{\rm eff}$, $\log g$, and [Fe/H], respectively, and mean offsets were small at 5 K, 0.00 dex, and 0.00 dex, respectively. We refer to the calibrated SpecMatch parameters hereafter.

3.2. SME@XSEDE

We also measured $T_{\rm eff}$, $\log g$, [Fe/H], and $V \sin i$ using SME@XSEDE, a set of Python routines wrapped around the widely-used spectral synthesis program, Spectroscopy Made Easy (SME; Valenti & Piskunov 1996). Stellar characterization with SME is done with the spectral synthesis technique which generates a synthetic spectrum that matches the observed data by performing radiative transfer through a model atmosphere based on a set of global stellar properties. SME@XSEDE

 $^{^{20}\ \}mathrm{https://github.com/petigura/specmatch-syn}$

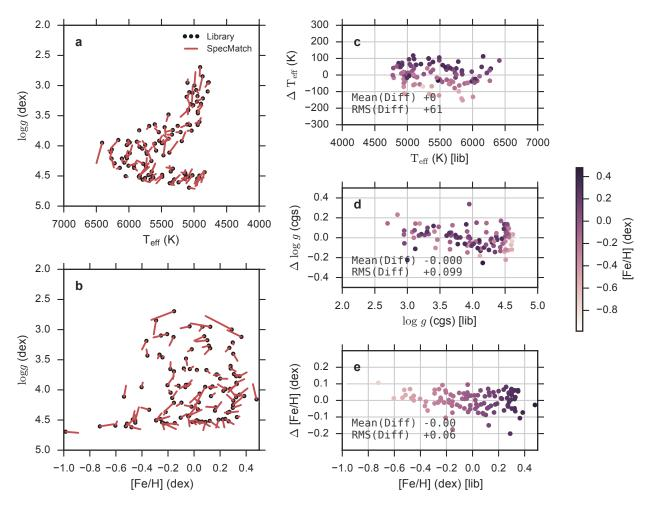


Fig. 3.— Comparison of stellar parameters from the Brewer et al. (2016) (B16) spectroscopic analysis and SpecMatch. a) Black points show $T_{\rm eff}$ and $\log g$ from B16 and red lines point to the SpecMatch values. Shorter lines correspond to tighter agreement. b) Same as a), except showing $\log g$ and [Fe/H]. c) Differences in $T_{\rm eff}$ between SpecMatch and B16, i.e. $\Delta T_{\rm eff} = T_{\rm eff}$ (SM) $-T_{\rm eff}$ (B16), as a function of $T_{\rm eff}$ (B16). Points are colored according to B16 metallicity d-e) Same as c), except showing $\log g$ and [Fe/H], respectively. Dispersion (RMS) in $\Delta T_{\rm eff}$, $\Delta \log g$, $\Delta [Fe/H]$ is 61 K, 0.099 (dex), 0.06 (dex), respectively. We note a residual correlation between $\Delta T_{\rm eff}$ and [Fe/H] in c) of \approx 10 K per 0.1 dex. For the sake of simplicity, we elected not to calibrate out this trend. The systematic is reflected in the 60 K (RMS) scatter in $\Delta T_{\rm eff}$ and in our adopted uncertainties of 60 K.

automates the process of spectral synthesis, facilitating the analysis of large data sets of high-resolution spectra in order to determine robust stellar parameters with realistic uncertainties in a hands-off fashion.

At its core, SME@XSEDE uses version 342 of the SME program. SME 342 has three main components: the radiative transfer engine, the software that interpolates the grid of model atmospheres, and the Levenberg-Marquardt non-linear least-squares solver that finds the optimal solution. As the SME 342 solver converges from the initial guesses to a set of best-fit free parameters, each step in the χ^2 minimization process requires an interpolation of the input model atmosphere grid at the specific set of global parameters, and then a new solution is found of the radiative transfer equations through this specific model atmosphere. SME 342 uses a fast radiative transfer algorithm based on the SYNTH code (Piskunov 1992). This employs an adaptive wavelength grid, in which the density of radiative transfer calculations is adjusted to increase the spectral resolution in the vicinity of absorption lines and decrease the resolution in regions of the continuum. The structure of stellar

atmospheres includes steep gradients with curvature of density, pressure, and temperature, therefore, SME 342 uses a specialized routine to perform non-linear Bezier interpolation of a grid of atmosphere models in order to predict a stellar atmosphere at a specific set of global stellar parameters.

SME@XSEDE requires as input (1) a set of planeparallel model atmospheres, (2) a list of atomic and molecular lines and their associated line parameters (i.e. a line list), and (3) initial guesses for the free parameters. When analyzing the CKS stars, SME@XSEDE ingests a grid of plane-parallel MARCS model atmospheres (Gustafsson et al. 2008) calculated under conditions of local thermodynamic equilibrium and spanning the range of potential stellar parameters in T_{eff} , $\log g$, and [Fe/H]. Since the model atmospheres have plane-parallel geometry and do not include a realistic treatment of convection, SME introduces the microturbulent and macroturbulent velocity parameters ($V_{\rm mic}$ and $V_{\rm mac}$, respectively) to achieve better agreement between the synthetic and observed spectra. In SME@XSEDE, we adopt empirical analytic functions for the behavior of the microand macroturbulent velocities that are dependent on $T_{\rm eff}$. Specifically, we use a relationship for the microturbulent velocity given by Gómez Maqueo Chew et al. (2013). For the macroturbulent velocity, we incorporate the relationship given by Valenti & Fischer (2005). We also note that instead of using one fixed velocity throughout the χ^2 minimization, we use dynamic values that are adjusted appropriately at each minimization step based on the effective temperature.

SME@XSEDE uses a line list and abundance pattern adapted from Stempels et al. (2007) and Hebb et al. (2009). This line list contains atomic and molecular transition information taken from the VALD database and the information provided on Robert Kurucz's website (Kurucz & Peytremann 1975). The wavelengths included in the spectral synthesis are the region around the Mg b triplet (5150-5200 Å), the NaI D doublet region (5850–5950 Å), and the wavelength region of 6000– 6200 Å which contains many isolated atomic lines and is relatively free of telluric features. We have incorporated the empirical corrections to the oscillator strengths and broadening parameters for individual lines determined by Stempels et al. (2007) through a comparison between a high-resolution spectrum of the Sun (Kurucz et al. 1984) and a synthetic spectrum calculated using the spectroscopic parameters of the Sun.

Like any Levenberg-Marquardt based solver, SME 342 requires a good initial guess and a smoothly varying χ^2 surface in order to consistently find the optimal solution at the absolute global minimum. Unfortunately, the discreteness of the wavelength and stellar atmosphere grids utilized by SME 342 add artificial structure to the χ^2 surface and hinder convergence. In addition, without a priori information about the free parameters, a single run of SME 342 can become stuck in a local minimum and fail to converge to the global solution. Historically, the χ^2 minimum has been found through hands-on manipulation by an expert SME user. SME@XSEDE solves this problem and automates the spectral synthesis process by running many realizations of SME 342 starting from different initial conditions. Due to the convergence issues with a single run of SME 342, the distribution of output solutions from the multiple trials performed by SME@XSEDE results in a sampling of the χ^2 surface close to the global minimum which SME@XSEDE uses to identify the best stellar parameters and their uncertainties (see Figure 4).

Using this approach, we analyzed 972/1305 CKS spectra on the Stampede computer cluster at NSF's XSEDE facility. (A few stars were not analyzed by SME@XSEDE because their spectra were not gathered when the computing time was available. SpecMatch parameters are available for those stars.) The automated SME@XSEDE run on each star includes 98 realizations of SME 342 started from a range of different initial conditions determined by randomly drawing from uniform distributions around the *Kepler* Input Catalog parameters for each star. After the initial SME@XSEDE run is complete, a further check is performed to insure that the distributions of output values is smaller and fully encompassed by the range of initial guesses. If not, SME@XSEDE was

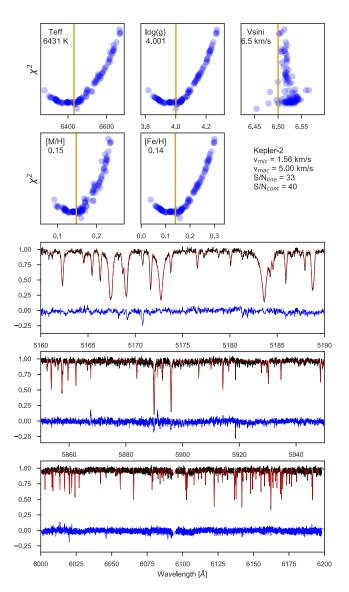


Fig. 4.— Output from SME@XSEDE for the CKS spectrum of Kepler-2. Top panels show for each global parameter the output distribution of χ^2 values for a set of initial guesses. The vertical lines show the determined best-fit parameters. The bottom three panels show observed spectrum (black), synthesized spectrum (red), and residuals (blue).

re-run with a wider range of initial guesses. This limits bias in final stellar parameters due to selecting only a small or systematically skewed set of initial guesses.

Figure 4 shows the output from an SME@XSEDE analysis of Kepler-2 (also known as HAT-P-7; Pál et al. 2008). The top five panels show the final χ^2 distribution versus each of the free parameters ($T_{\rm eff}$, $\log g$, [Fe/H], $V \sin i$, and [M/H]) resulting from the 98 independent realizations of SME 342. The majority of runs do not converge to the global χ^2 minimum, but the resulting distribution of final values describes the χ^2 surface which we use to determine the optimal parameter values at the global minimum (dark tan line) and the asymmetric 1σ uncertainties on these values (light tan region). The bottom three panels show the observed spectrum in the synthesis regions (black) with the best fitting synthetic spectrum over-plotted (red).

 $^{^{21}}$ With the sign correction specified in Footnote 6 of (Torres et al. 2012)

4. CATALOG OF STELLAR PROPERTIES

We compared the outputs of the two different codes, SpecMatch and SME@XSEDE. For our final results, we combined the parameters produced by both codes, after making small adjustments to the raw SME@XSEDE values to place them on the SpecMatch scale. Figure 6 shows the spectroscopic HR diagram $(T_{\rm eff}, \log g)$ for the SpecMatch, SME@XSEDE, and combined catalogs. Figures 6 and 7 show projections of the parameters into the $(T_{\rm eff}, [{\rm Fe/H}])$ and $([{\rm Fe/H}], \log g)$ planes. We describe our procedure for combining the two spectroscopic catalogs below.

4.1. SpecMatch and SME@XSEDE Catalogs

The catalogs of stellar properties produced by SpecMatch and SME@XSEDE show excellent agreement in $T_{\rm eff}$, $\log g$, and [Fe/H] for stars that are not deemed false positives. Figure 8 shows the differences between the raw results from the two pipelines, analyzing the same stellar spectrum. The systematic differences in T_{eff} , $\log g$, and [Fe/H] determinations are small, with median and RMS differences between SpecMatch and SME@XSEDE analyses of the same stellar spectra being comparable to the individual measurement errors. We correct for the small systematic differences as described below. The independent $V \sin i$ measurements do not agree, however. This is due to the use of a Gaussian instrumental profile with a resolution of $R \sim 75,000$ in SME@XSEDE, which is higher than the empirically-determined value used in SpecMatch. Because of this known systematic issue in the $V \sin i$ values from SME@XSEDE, we adopt the SpecMatch values of $V \sin i$ for all stars in this catalog.

4.2. Calibration of SME@XSEDE Parameters

We attempted to correct the low-order differences between the SpecMatch and SME@XSEDE parameters to put the catalogs on the same scale. We adopted SpecMatch as the standard since it is well-calibrated for all parameters. In addition, a comparison of the $V\sin i$ values for 43 stars with Rossiter-McLaughlin of transiting giant planets (Albrecht et al. 2012) and SpecMatch analyses showed agreement at the level of 1 km s $^{-1}$ (RMS). Because of this heritage, we made minor corrections to the SME@XSEDE parameter values and left the SpecMatch values unchanged.

We compare the differences between the SpecMatch and SME@XSEDE parameters in Figure 8. Following the methodology of Section 3.1, we derived a correction that calibrates the SME@XSEDE parameters onto the SpecMatch (and B16 scale) via $SX_{cal} = SX_{raw} + \Delta$. The corrections are linear (and therefore continuous) functions of the following form:

$$\begin{split} \Delta T_{\rm eff} &= a_0 + a_1 \left(\frac{T_{\rm eff} - 5500 \text{ K}}{100 \text{ K}} \right), \\ \Delta \log g &= b_0 + b_1 \left(\frac{\log g - 3.5 \text{ dex}}{0.1 \text{ dex}} \right), \\ \Delta [\text{Fe/H}] &= c_0 + c_1 \left(\frac{[\text{Fe/H}]}{0.1 \text{ dex}} \right), \end{split}$$

where $a_0 = -28.7$ K and $a_1 = -5.17$; $b_0 = 0.0146$ dex, $b_1 = 0.0028$, $c_0 = 0.0034$ dex, and $c_1 = -0.0175$. After

applying these corrections, we compare the calibrated SME@XSEDE and SpecMatch parameters in Figure 9. We find a dispersion of 68 K, 0.09 dex, and 0.036 dex in $T_{\rm eff}$, log g, [Fe/H], respectively.

4.3. Parameter Averaging

One of the key features of the CKS catalog is that three quarters of the spectra (972/1305) were analyzed by two independent spectral analysis pipelines. This enables the straightforward identification of suspect spectroscopic parameters where the two techniques produce disparate results. For stars with consisent parameters from both catalogs, we adopted the arithmetic mean the SpecMatch and SME@XSEDE values for $T_{\rm eff}$, $\log g$, and [Fe/H]. We adopted the SpecMatch $V \sin i$ values for all stars. For a small number of stars, we rejected the parameter values determined by one of the two pipelines; these cases are described below. The distributions of adopted values of $T_{\rm eff}$, $\log g$, [Fe/H], and $V \sin i$ are shown in Figure 10.

4.4. Outlier Rejection

Determining parameters from two pipelines offers the opportunity to discover cases of significant disagreement. We identify 26 stars where any of the following conditions are satisfied: (1) $T_{\rm eff}$ differed by more than 300 K, (2) $\log g$ differed by more than 0.35 dex, or (3) [Fe/H] differed by more than 0.30 dex. These stars are highlighted in Figure 8 and are marked with a flag in the machine-readable version of Table 5. We recommend excluding these stars from further statistical analyses.

In anticipation of studies where a preferred value for one or more of these stars is needed, we inspected the parameters from SpecMatch and SME@XSEDE. In cases where one pipeline clearly failed, we adopted the triplet of parameters ($T_{\rm eff}$, $\log g$, [Fe/H]) determined by the other method. Figures 6–7 show the spectroscopic parameters in three planes. Outliers can be identified by dashed lines with red points marking the adopted values.

The KIC (Brown et al. 2011) offers a third determination of effective temperature (see Sec. 5.1). For cases of >300 K disagreement between SpecMatch and SME@XSEDE, we adopted $T_{\rm eff}$ from the pipeline closest matching to the KIC value. We adopted the SpecMatch parameters for KOI-156, KOI-719, KOI-935, KOI-3683, KOI-4060. For KOI-870, we choose the SpecMatch value because the mean stellar density determined from the transit light curve is nearer to that implied by the SpecMatch parameters. For KOI-1054, we adopted the SME@XSEDE value because those parameters more closely match the KIC parameters.

For cases where $\log g$ disagreed by >0.35 dex, we adopted the parameter that most closely matched a previously published result, when available. We adopted SpecMatch values for KOI-3, KOI-104, KOI-1963, KOI-4601, KOI-4651, KOI-4699.

For cases with significant $\log g$ disagreement, but lacking existing literature values, we inspected the combinations of $T_{\rm eff}$ and $\log g$ returned by SpecMatch and SME@XSEDE and searched for cases where one pipeline gave values that are inconsistent with the observed properties of normal stars (e.g. Torres et al. 2010). We adopt SpecMatch parameters for the following stars KOI-2287,

KOI-2503, and KOI-3928 because the SME@XSEDE parameters constitute unphysical combinations of $T_{\rm eff}$ and $\log g$.

Finally, for KOI-193, KOI-2228, KOI-2481, KOI-2676, KOI-2786, KOI-3203, KOI-3215, KOI-3419, and KOI-4053 there was no clear indication of a failure in either of the pipelines, so we simply averaged the parameters.

4.5. Adopted Values

Table 5 lists the adopted values $T_{\rm eff}$, $\log g$, [Fe/H], and $V \sin i$, as well as individual determinations by the SpecMatch and SME@XSEDE pipelines. We also list radial velocities relative to the barycenter of the solar system, having accuracies of 0.1 km s⁻¹, determined using the method of Chubak et al. (2012).

4.6. Precise Validation with Platinum Sample

All methods to determine spectroscopic parameters have some systematic and random errors. We use two methods, asteroseismology and line-by-line spectroscopic synthesis, as validation standards against which we calibrate the CKS results. These results are summarized in Table 7.

4.6.1. Huber et al. (2013)

Huber et al. (2013) measured the properties of 77 planet host stars using Kepler asteroseismology. The asteroseismic analysis is much more precise than our spectroscopic method in $\log g$ determination and is only modestly sensitive to the input values of $T_{\rm eff}$ and [Fe/H], which were measured by the SPC method (Buchhave et al. 2012). As described in Petigura (2015), we used 71 of the stars in the Huber et al. (2013) sample to compare with our CKS results. Figure 11 compares the spectroscopic parameters for the stars in common between CKS and Huber et al. (2013). We find excellent agreement in $\log g$ with an offset of -0.03 dex and an RMS of 0.08 dex between the two measurement techniques. This tight agreement between asteroseismology and CKS supports the 0.10 dex adopted uncertainty for the CKS $\log g$ values

For the lowest gravity stars in the comparison, we note a systematic trend in $\Delta \log g$. At $\log g = 3.2$ dex, the CKS gravities are 0.2 dex larger than the Huber et al. (2013) values. This trend may be due in part to discrepancies between the B16 spectroscopic gravities and asteroseismic gravities for evolved stars. B16 demonstrated 0.05 dex (RMS) agreement with asteroseismology for a sample of 42 Kepler stars with $\log g = 3.7-4.5$ dex. Thus, the B16 gravities may be offset from asterosiesmic gravities for stars with $\log g < 3.7$ dex. This systematic trend affects only small subset of the CKS sample. The vast majority (97%) the stars are high gravity ($\log g > 3.7$ dex), where we see excellent agreement with asteroseismology.

4.6.2. Bruntt et al. (2012)

As a second validation sample, we used the results for the 93 "platinum stars" identified and analyzed by the Kepler Project to establish stellar parameters of the highest possible accuracy. These 93 stars are all bright and were subjects of asteroseismic and spectroscopic analyses. Bruntt et al. (2012) (B12) gathered high-resolution (R=80,000), high S/N (200-300 per pixel) spectra of these solar type stars using the ESPaDOnS spectrograph on the 3.6-m Canada-France-Hawaii Telescope. They used the VWA (Bruntt et al. 2010) analysis tool to perform an iterative, line-by-line spectroscopic synthesis to match the observed spectra. This tool has itself been calibrated on samples with asteroseismic and interferometric measurements. The spectroscopic fits were done with $\log g$ held fixed to values determined by asteroseismic analysis of Kepler photometry (Verner et al. 2011a,b).

Figure 12 compares the spectroscopic parameters for 57 stars in common between SpecMatch and (B12). Note that these stars are generally not the hosts of transiting planets, and thus are not part of the CKS sample. The HIRES spectra for this comparison were gathered separately. The parameters $T_{\rm eff}$, $\log g$ and [Fe/H] all show good agreement with negligible offsets and low scatter. This establishes the precision and accuracy of SpecMatch and CKS (see Sec. 4.7 and Table 6).

$4.7. \ Uncertainties$

We adopt a precision of 60 K for $T_{\rm eff}$ for comparison within this catalog. This is based on the 60 K agreement between SpecMatch and Brewer et al. (2016) (B16) temperatures. Because of systematic differences between $T_{\rm eff}$ scales between catalogs (see e.g. Pinsonneault et al. 2012; Brewer et al. 2016), we encourage adding 100 K systematic uncertainty in quadrature (116 K total uncertainty) for applications beyond internal comparisons within the CKS catalog.

We adopt a $\log g$ uncertainty in this catalog of 0.10 dex based on the agreement between SpecMatch and B16 surface gravities. This is supported by the 0.09 dex agreement between SpecMatch and SME@XSEDE gravities (Figure 9) as well as the agreement with asteroseismic gravities, presented in Sections 4.6.1 and 4.6.2.

For spectroscopic analyses, modeling uncertainties such as incomplete or inaccurate line lists, imperfect model atmospheres, and the assumption of LTE will influence the derived $T_{\rm eff}$, $\log g$, and [Fe/H]. For $T_{\rm eff}$ and $\log g$, there are independent measurement techniques that yield parameters with precisions and accuracies that are comparable to, or higher than, those from spectroscopy. Examples include the Infrared Flux Method (IRFM) for $T_{\rm eff}$ and asteroseismology for $\log g$. These independent techniques are often used to characterize the modeling uncertainties associated with spectroscopy.

Characterizing the effect of modeling uncertainties on spectroscopic metallicities is challenging because there are no non-spectroscopy techniques with comparable precision/accuracy that can serve to validate the spectroscopic metallicities. A standard method to quantify such errors is to compare metallicities derived through different codes with the assumption that the model-dependent uncertainties are reflected in the scatter and offsets between the two techniques.

We note the agreement between metallicities derived through four different techniques that all analyzed high resolution, high SNR spectra. SpecMatch, SME@XSEDE, B16, and B12 used a variety of line lists, radiative transfer codes, and model atmospheres. We observe a 0.036 dex scatter between SpecMatch and SME@XSEDE metallicities and a 0.06 dex scatter between SpecMatch and B16 metallicities.

The metallicities of both SpecMatch and SME@XSEDE were placed onto the B16 scale, so there are no mean offsets by construction. However, in comparing SM to B12, we note a slight deviation from the 1-to-1 line and a mean offset of 0.056 dex. This reflects different metallicity scales associated with the B16 and B12 analyses, which likely stem from different line lists, model atmospheres, radiative transfer codes, etc.

We adopt a metallicity precision of 0.04 dex for comparison within this catalog motivated by the SpecMatch-SME@XSEDE agreement. Because of systematic differences between the B16 and B12 metallicity scales, we encourage adding 0.06 dex systematic uncertainty in quadrature (0.07 dex total uncertainty) for applications beyond internal comparisons within the CKS catalog.

The $V \sin i$ values are entirely determined from SpecMatch. We adopt 1- σ errors of 1 km s⁻¹ and an upper limit of 2 km s⁻¹ for stars with $V \sin i < 1$ km s⁻¹. This uncertainty is based on a comparison of $V \sin i$ values determined by Rossiter-McLaughlin measurements (Albrecht et al. 2012) to the SpecMatch-determined values for the same stars (Petigura 2015).

5. COMPARISON WITH OTHER SURVEYS OF KEPLER PLANET HOSTS

Table 7 provides a comparison between CKS results and several surveys of KOIs, described below.

5.1. Kepler Input Catalog

The Kepler Input Catalog (KIC; Brown et al. 2011) was constructed prior to the launch of Kepler from griz+Mg b photometry. It was well suited for the purpose of selecting appropriate stars to be monitored by the spacecraft photometer. The KIC has stated uncertainties of 200 K in $T_{\rm eff}$ and 0.4 dex in $\log g$ (both for $T_{\rm eff}$ in the range 4500-6500 K). Metallicity ($\log(Z)$) was reported, but the uncertainties were expected to be high. While the KIC was used with great success to select dwarf Sunlike stars for the mission, it did not provide reliable surface gravity and metallicity measurements. This was one of the primary motivations of the CKS project. Figure 12 compares the CKS stellar parameters to the KIC.

5.2. Huber et al. (2014)

Huber et al. (2014) provided a comprehensive update to the KIC by compiling literature measurements of stellar properties from different observational techniques (photometry, spectroscopy, asteroseismology, and exoplanet transits) and homogeneously fitting them to a grid of Dartmouth stellar isochrones. This often allowed the uncertainties in the stellar parameters to be reduced, in comparison to the KIC. For the 1244 stars analyzed by Huber et al. (2014) for which we have spectroscopy, their stated uncertainties are 2–3.5% (fractional) in $T_{\rm eff}$, 0.40 dex to 0.15 dex in $\log g$, and 0.30 to 0.15 dex in [Fe/H], all considerably larger than the CKS errors here. Figure 14 compares the SpecMatch and Huber et al. (2014) values.

5.3. LAMOST

The Large Sky Area Multi-Object Fiber Spectroscopic Telescope (LAMOST; Luo et al. 2015; Dong et al. 2014) is instrumented with highly-multiplexed (4000 fibers per 5 degree field), low-resolution (R=1000 or 5000) spectrometer. It can cover the entire Kepler Field in 14 pointings. LAMOST is engaged in several large spectroscopic surveys, including a set of 6500 asteroseismic targets and $\sim 150,000$ "planet targets" in the Kepler Field. The LAMOST Stellar Parameter (LASP; Luo et al. 2015; Wu et al. 2014) pipeline is used to compute $T_{\rm eff}$, log g, and [Fe/H], which are stored in a large catalog (De Cat et al. 2015). The stated uncertainties for LAMOST are typically 100 K in $T_{\rm eff}$, 0.10 dex in $\log g$, and 0.10 dex in [Fe/H]. In Figure 15 we compare SpecMatch and LAMOST results.

5.4. SPC

The Stellar Parameter Classification (SPC; Buchhave et al. 2012, 2014; Buchhave & Latham 2015) tool matches observed high-resolution spectra to a library grid of synthetic model spectra using a prior on $\log g$ from stellar evolutionary models. The stated uncertainties for SPC are typically 50 K in $T_{\rm eff}$, 0.10 dex in $\log g$, and 0.08 dex in [Fe/H]. Figure 16 compares SpecMatch and SPC results. The SPC results are from FIES, TRES, and HIRES spectra (Buchhave et al. 2014).

5.5. KEA

KEA (Endl & Cochran 2016) is a spectral analysis tool that uses a large grid of model stellar spectra (Kurucz 1993) computed with an LTE spectrum synthesis (Sneden 1973). KEA was calibrated on Kepler "platinum stars" and has stated uncertainties of 200 K in $T_{\rm eff}$, 0.18 dex in log g, and 0.12 dex in [Fe/H]. Figure 17 compares results from SpecMatch and KEA-analyzed spectra from McDonald Observatory. The comparison with CKS is limited in usefulness because of only 44 stars in common that span a relatively narrow range of log g and [Fe/H].

5.6. Everett et al. (2013)

Everett et al. (2013) measured low-resolution (R=3000) optical spectra of 268 stars using the National Optical Astronomy Observatory (NOAO) Mayall 4 m telescope on Kitt Peak and the facility RCSpec long-slit spectrograph. They report uncertainties of 75 K in $T_{\rm eff}$, 0.15 dex in $\log g$, and 0.10 dex in [Fe/H]. Figure 18 compares CKS and Everett et al. (2013). Note the systematic trends in $\log g$ and [Fe/H] in the comparison plots.

5.7. Flicker

Bastien et al. (2013) developed a method to measure $\log g$ using Kepler light curves themselves. "Flicker" measures photometric variability from convective granulation on short timescales. It works because the amplitude of convective granulation depends on the strength of the restoring force, i.e., surface gravity. Bastien et al. (2014) noted that Flicker-based gravities were systematically higher than those in the KIC, implying that most Kepler planets (which lacked spectroscopically-determined gravities) had radii that were underestimated by 20-30%. Bastien et al. (2016) improved the Flicker

 $^{^{22}\,}$ Brown et al. (2011) states, "it is difficult to assess the reliability of our $\log(Z)$ estimates, but there is reason to suspect that it is poor, particularly at extreme $T_{\rm eff}$."

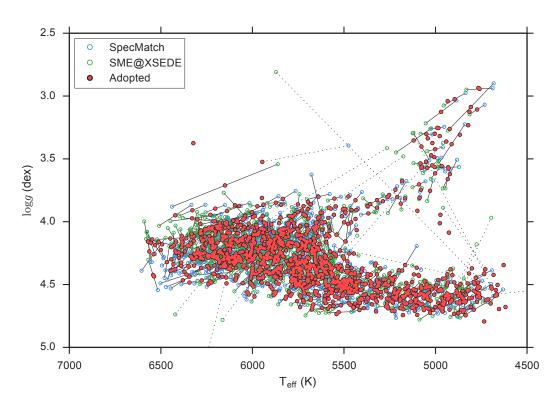


Fig. 5.— Hertzsprung-Russell diagram (log g versus $T_{\rm eff}$) for CKS stars. Blue points are parameter values from SpecMatch, green are from SME@XSEDE, and red are the adopted values. Solid lines connect SpecMatch and SME@XSEDE values for the same star, for cases in which simple averaging of the results of the two methods was applied. Dashed lines connect SpecMatch and SME@XSEDE values for which the results of one method was rejected and the other was adopted. SME@XSEDE values have been corrected to be on the SpecMatch scale (Sec. 4.2).

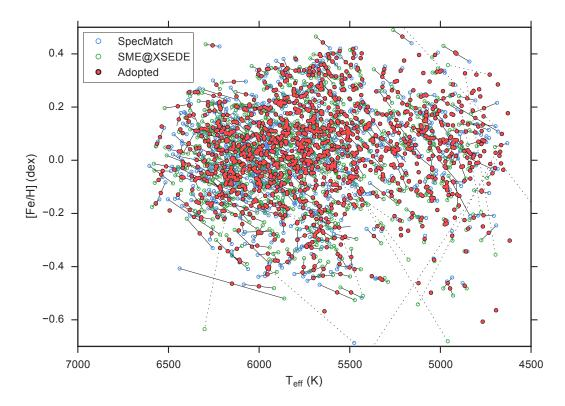


Fig. 6.— Same as Figure 6 except the axes are $T_{\rm eff}$ and [Fe/H].

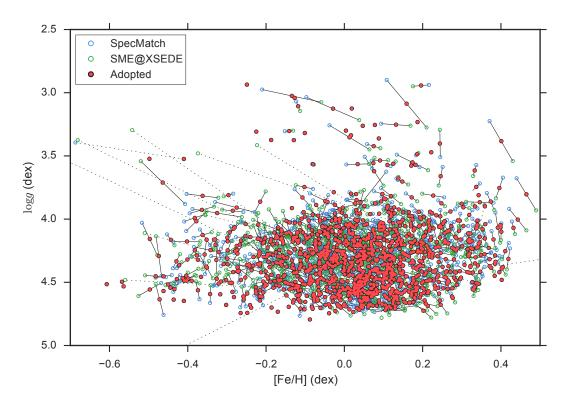


Fig. 7.— Same as Figure 6 except the axes are [Fe/H] and $\log g$.

 $\begin{array}{c} {\rm TABLE~5} \\ {\rm Spectroscopic~Parameters} \end{array}$

-	Adopted Values				Adopted Values SpecMatch				SME@XSEDE				_	
KOI No.	T_{eff} (K)	$\log g$ (dex)	$[{\rm Fe/H}] \\ ({\rm dex})$	$V\sin i \\ (\mathrm{km}\mathrm{s}^{-1})$	$T_{\rm eff}$ (K)	$\log g$ (dex)	$[{\rm Fe/H}] \\ ({\rm dex})$	$V\sin i \\ (\mathrm{km}\mathrm{s}^{-1})$	$T_{\rm eff}$ (K)	$\log g$ (dex)	$[{\rm Fe/H}] \\ ({\rm dex})$	$V\sin i \\ (\mathrm{km}\mathrm{s}^{-1})$	${\rm TRV} \atop ({\rm kms^{-1}})$	
K00001 K00002	5819 6449	4.40 4.13	$+0.01 \\ +0.20$	1.3 5.2	5853 6376	4.43 4.13	$+0.02 \\ +0.21$	1.3 5.2	5785 6521	4.37 4.14	$+0.01 \\ +0.20$	4.3 6.1	$+0.5 \\ -10.4$	
K00003 K00006 K00007	4864 6348 5827	4.50 4.36 4.09	+0.33 +0.04 +0.18	$3.2 \\ 11.8 \\ 2.8$	4864 6348 5813	4.50 4.36 4.03	+0.33 +0.04 +0.17	$3.2 \\ 11.8 \\ 2.8$	4696 5841	3.97 4.15	-0.36 $+0.18$	3.1 4.6	-63.4 -42.8 -60.8	

Note. — Adopted Values are our best determination of the spectroscopic parameters after calibrating the SME@XSEDE values and averaging with the SpecMatch values. Uncertainties for the Adopted Values are summarized in Table 6 and Section 4.7. Results from SME@XSEDE (after the calibrations described in Section 4.2) and SpecMatch are also presented. This table will be published in its entirety in the machine-readable format in the accepted version of this paper. A portion is shown here for guidance regarding its form and content.

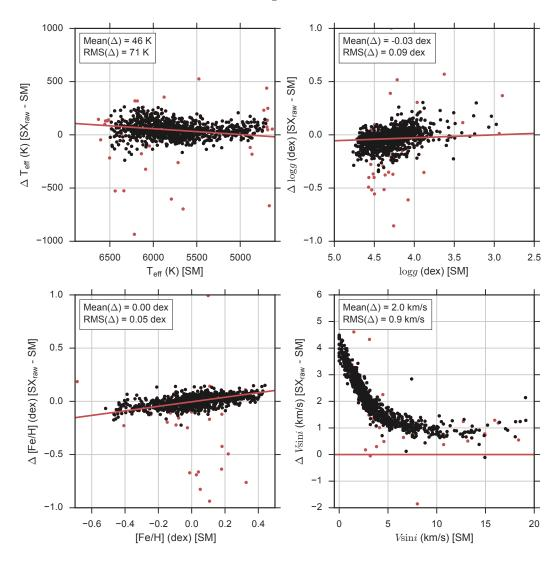


Fig. 8.— Four panels showing the differences in stellar parameters determined independently by the SpecMatch (SM) and SME@XSEDE (SX_{raw}) algorithms. Panels correspond to $T_{\rm eff}$ (upper left), $\log g$ (upper right), [Fe/H] (lower right), and $V \sin i$ (lower right). Each panel shows the difference between the SM and raw SX parameter values for each star, as a function of the SM values. Annotations give the mean and RMS differences between the SM and uncalibrated SX catalogs. Red lines show the corrections that were applied to SX parameter values (see Sec. 4.2). Subsequent figures show SX parameter values with these corrections applied. We have highlighted the 26 stars where significant disagreement exists between the two methods see Sec. 4.4. These stars are excluded from the calibrations and subsequent analyses.

TABLE 6
Adopted Parameter Uncertainties

Parameter	1-σ Uncertainty
$T_{ m eff}$	±60 K (relative; within this catalog) ±100 K (systematic)
$\log g$ [Fe/H]	±0.10 dex ±0.04 dex (relative; within this catalog) ±0.04 dex (systematic)
$V \sin i$	$\pm 1 \text{ km s}^{-1}$ < 2 km s^{-1} upper limit for $V \sin i < 1 \text{ km s}^{-1}$

method by measuring photometric variability on multiple timescales, but excluded KOIs from their catalog. Figure 19 compares CKS and Bastien et al. (2014) $\log g$ performance for stars brighter than Kp=13. As noted in Bastien et al. (2016), Flicker performs best for the brightest stars with the lowest photon-limited noise.

6. SUMMARY AND DISCUSSION

We present precise stellar parameters ($T_{\rm eff}$, $\log g$, [Fe/H], and $V \sin i$) for 1305 Kepler planet host stars based on a uniform set of high-S/N, high-resolution spectra from Keck/HIRES. Our magnitude-limited (Kp < 14.2) CKS sample, augmented with multi-planet systems and other planet samples, constitutes the largest set of stars and transiting planets with precisely determined stellar parameters to date.

Stellar parameters were determined using two methods, SpecMatch and SME@XSEDE. The zero-points and scales of our measurements are calibrated against "platinum star" samples observed with higher precision methods (asteroseismology and line-by-line spectral synthesis applied to high-S/N spectra). The uncertainties of our adopted parameters are 60 K in $T_{\rm eff}$, 0.10 dex in $\log g$, 60 dex in [Fe/H], and 1 km s⁻¹ in $V \sin i$.

We find that the *Kepler* planet host stars have distri-

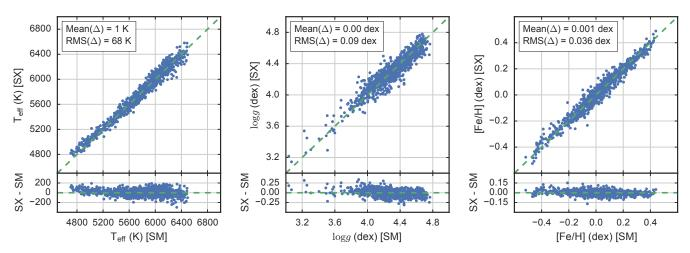


Fig. 9.— Comparison of SpecMatch (SM) and SME@XSEDE (SX) values for $T_{\rm eff}$, $\log g$, and [Fe/H]. The SME@XSEDE values have been adjusted to the SpecMatch scale (Sec. 4.3). The top panel compares SM and SX parameters while the lower panel shows their difference as a function of the SM parameters. Equality between SM and SX are shown as green lines. The RMS value is the standard deviation of difference between SM and SX values for the same star.

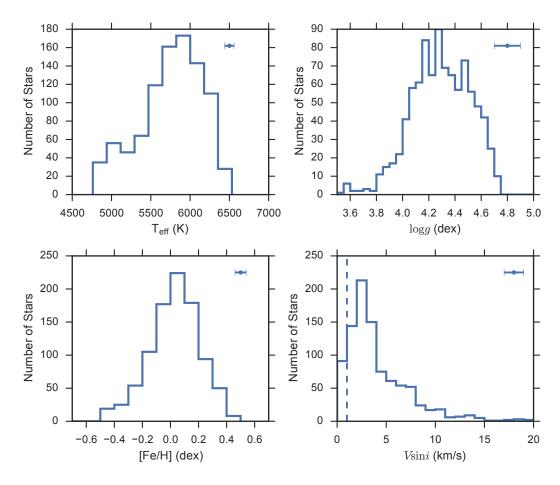


Fig. 10.— Histograms of the adopted spectroscopic parameters $(T_{\rm eff}, \log g, [{\rm Fe/H}] \text{ and } V \sin i)$ for all stars in our CKS sample. Adopted uncertainties (Table 6) are plotted in the upper right corner of each panel. $V \sin i$ is difficult to measure for the most slowly rotating stars. Thus we adopt 2 km s^{-1} as an upper limit for stars with reported $V \sin i < 1 \text{ km s}^{-1}$ (dashed line).

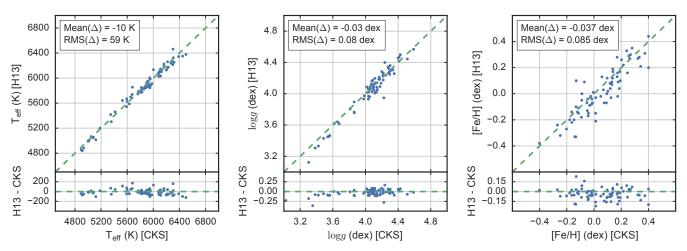


Fig. 11.— Comparison of $T_{\rm eff}$ (left), log g (middle), and [Fe/H] (right) values between CKS and Huber et al. (2013) (H13) asteroseismic analysis for 71 stars in common. Annotations indicate the mean and RMS differences between the samples.

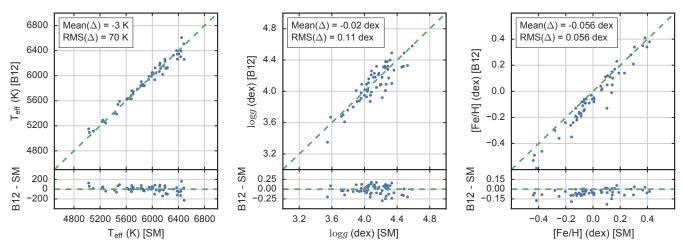


Fig. 12.— Comparison of $T_{\rm eff}$ (left), $\log g$ (middle), and [Fe/H] (right) values between SpecMatch (SM) and Bruntt et al. (2012) (B12) for 57 stars in common. Annotations indicate the mean and RMS differences between the samples.

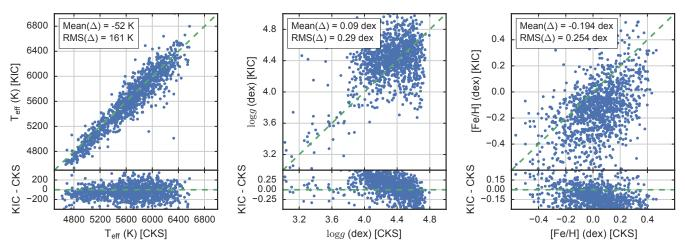


Fig. 13.— Comparison of $T_{\rm eff}$ (left), $\log g$ (middle), and [Fe/H] (right) values between CKS and Kepler Input Catalog (KIC; Brown et al. 2011) for 1215 stars in common. Annotations indicate the mean and RMS differences between the samples.

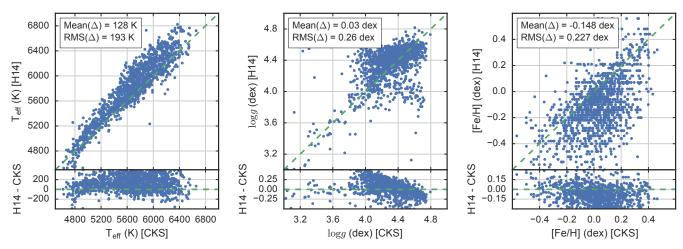


Fig. 14.— Comparison of $T_{\rm eff}$ (left), $\log g$ (middle), and [Fe/H] (right) values between CKS and the revised stellar properties from the Kepler team (H14; Huber et al. 2014) for 1302 stars in common. Annotations indicate the mean and RMS differences between the samples.

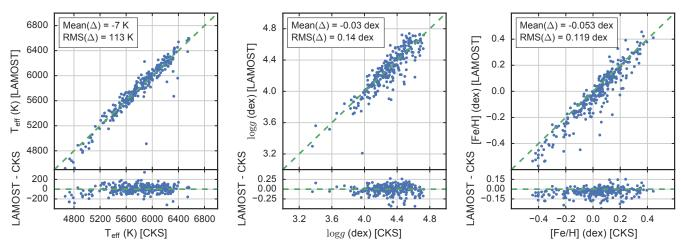


Fig. 15.— Comparison of $T_{\rm eff}$ (left), $\log g$ (middle), and [Fe/H] (right) values between CKS and the LAMOST survey (De Cat et al. 2015) for 283 stars in common. Annotations indicate the mean and RMS differences between the samples.

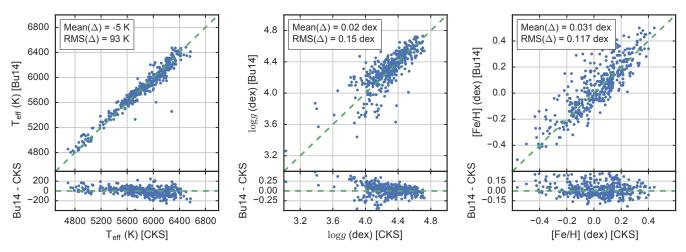


Fig. 16.— Comparison of $T_{\rm eff}$ (left), log g (middle), and [Fe/H] (right) values between CKS and analysis for high-resolution spectroscopy using SPC (Bu14; Buchhave et al. 2014) for 396 stars in common. Annotations indicate the mean and RMS differences between the samples.

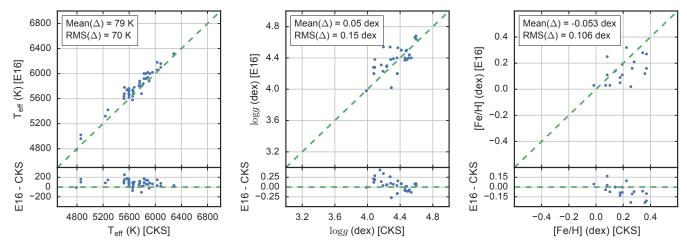


Fig. 17.— Comparison of $T_{\rm eff}$ (left), log g (middle), and [Fe/H] (right) values between CKS and analysis for high-resolution spectroscopy using KEA (E16; Endl & Cochran 2016) for 44 stars in common. Annotations indicate the mean and RMS differences between the samples.

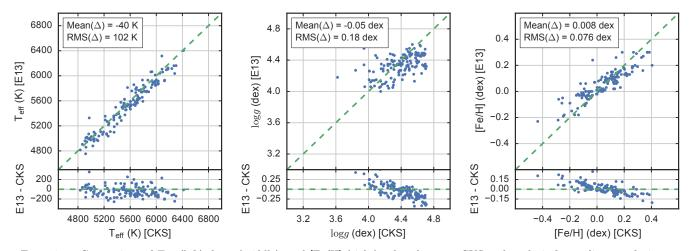


Fig. 18.— Comparison of $T_{\rm eff}$ (left), $\log g$ (middle), and [Fe/H] (right) values between CKS and analysis for medium-resolution spectroscopy by (E13; Everett et al. 2013) for 143 stars in common. Annotations indicate the mean and RMS differences between the samples.

	Sta	ted Uncertai	nties	_	Offset with CKS			RMS with CKS			
Catalog	$T_{ m eff}$ [K]	$\log g$ [dex]	[Fe/H] [dex]	N_{\star} common	$T_{\rm eff}$ [K]	$\log g$ [dex]	[Fe/H] [dex]	$\begin{array}{c} T_{\rm eff} \\ [{\rm K}] \end{array}$	$\log g$ [dex]	[Fe/H] [dex]	
This Paper											
CKS ^a	60 (rel) 100 (sys)	0.10	0.04 (rel) 0.06 (sys)								
Validation of CKS with Platinum St	ars										
Huber et al. $(2013)^{b}$ Bruntt et al. $(2012)^{c}$	 60	$0.01 \\ 0.03$	0.06	71 57	 -3	$-0.03 \\ 0.02$	-0.056	 70	$0.08 \\ 0.11$	 0.056	
Comparison Surveys											
KIC (Brown et al. 2011) ^d	200	0.40	$\sim \! 0.30$	1215	-52	+0.09	-0.194	161	0.29	0.254	
Huber et al. (2014) $^{\rm e}$	110 (sp) 193 (ph)	$0.15 \text{ (sp)} \\ 0.40 \text{ (ph)}$	$0.15 \text{ (sp)} \\ 0.30 \text{ (ph)}$	1302	+128	+0.03	-0.148	193	0.26	0.227	
LAMOST (De Cat et al. 2015)	100	0.10	0.10	283	-7	-0.03	-0.053	113	0.14	0.119	
SPC (Buchhave et al. 2014)	50	0.10	0.08	396	-5	+0.02	+0.031	93	0.15	0.117	
KEA (Endl & Cochran 2016)	100	0.18	0.12	44	+79	+0.05	-0.053	70	0.15	0.106	
Everett et al. (2013)	75	0.15	0.10	143	-40	0.05	+0.008	102	0.18	0.076	
Flicker (Bastien et al. 2014) f		0.10		232		-0.11			0.21		

TABLE 7 Comparison with Other Surveys

^f Flicker $\log g$ uncertainties are higher that 0.10 dex for some stars.

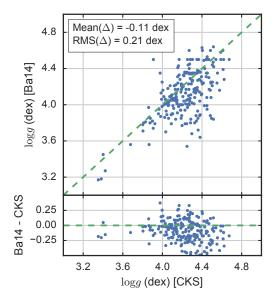


Fig. 19.— Comparison of $\log g$ values between CKS and the Flicker method (Ba14; Bastien et al. 2014) for 232 stars in common. Annotations indicate the mean and RMS differences between the samples.

butions of $T_{\rm eff}$, $\log g$, [Fe/H], and $V \sin i$ and an H-R Diagram that are similar to those of stars in the solar neighborhood, given the selection effects from the planet detection process of Kepler. In particular, for the magnitude-limited sample (Kp < 14.2), our CKS parameters give a median metallicity for Kepler planet host stars of -0.01 dex and an RMS of 0.19 dex. Valenti & Fischer (2005) measured the solar neighborhood to have a median metallicity of 0.00 dex and an RMS of 0.24 dex.

Additional CKS papers build on this work. In Paper II (Johnson et al., submitted), we compute precise stellar radii and masses, and approximate stellar ages. Paper III (Fulton et al., submitted) examines the planet radius distribution using our precise stellar radii and the planet-to-star radius ratios from *Kepler* photometry. Paper IV (Petigura et al., to be submitted) examines the metallicities of stars in the CKS sample. Paper V (Weiss et al., to be submitted) probes the similarities and differences in planetary and stellar properties for single and multi-planet transiting systems.

Facilities: Keck:I (HIRES), Kepler

The CKS project was conceived, planned, and initiated by AWH, GWM, JAJ, HTI, and TDM. AWH, GWM, JAJ acquired Keck telescope time to conduct the magnitude-limited survey. Keck time for the other stellar samples was acquired by JNW, LAR, and GWM. The observations were coordinated by HTI and AWH and carried out by AWH, HTI, GWM, JAJ, TDM, BJF, LMW, EAP, ES, and LAH. AWH secured CKS project funding. SpecMatch was developed and run by EAP and SME@XSEDE was developed and run by LH and PAC. Downstream data products were developed by EAP, HTI, and BJF. Results from the two pipelines were consolidated and the integrity of the parameters were verified by AWH, HTI, EAP, GWM, with assistance from BJF, LMW, ES, LAH, and IJMC. This manuscript was largely written by AWH and EAP with significant assistance from HTI, JNW, and GWM.

We thank Jason Rowe, Dan Huber, Jeff Valenti, Natalie Batalha, and David Ciardi for helpful conversations and Roberto Sanchis-Ojeda for his work on the Ultra-Short Period planet sample. We thank the many ob-

 $^{^{\}mathrm{a}}$ CKS uncertainties in T_{eff} are 60 K within the sample (rel) and 100 K systematic uncertainty (sys) when compared to other surveys.

^b Huber et al. (2013) is a platinum sample for $\log g$ measurements only, using asteroseismology. $T_{\rm eff}$ and [Fe/H] for this sample are based on SPC; see Sec. 4.6.1.

^c The comparison with Bruntt et al. (2012) is with SpecMatch parameters, not SME@XSEDE or their combination, CKS.

 $^{^{\}rm d}$ Errors for the KIC are for $T_{\rm eff}$ in the range 4500–6500 K.

^e Errors for Huber et al. (2014) are specified separately for stars with photometry (ph) or also spectroscopy (sp). $T_{\rm eff}$ errors are stated as 3.5% (193 K at 5500 K) for photometry and 2% (110 K at 5500 K) for spectroscopy.

servers who contributed to the measurements reported here. PAC and LH thank Jeff Valenti, and Eric Stempels for their extensive help in running SME and developing the SME implementation presented in this paper. We gratefully acknowledge the efforts and dedication of the Keck Observatory staff, especially Randy Campbell, Scott Dahm, Greg Doppmann, Marc Kassis, Jim Lyke, Hien Tran, Josh Walawender, Greg Wirth for support of HIRES and of remote observing. Most of the data presented herein were obtained at the W. M. Keck Observatory, which is operated as a scientific partnership among the California Institute of Technology, the University of California, and NASA. We are grateful to the time assignment committees of the University of Hawaii, the University of California, the California Institute of Technology, and NASA for their generous allocations of observing time that enabled this large project. Kepler was competitively selected as the tenth NASA Discovery mission. Funding for this mission is provided by the NASA Science Mission Directorate. We thank the Kepler Science Office, the Science Operations Center, Threshold Crossing Event Review Team (TCERT), and the Follow-up Observations Program (FOP) Working Group for their work on all steps in the planet discovery process ranging from selecting target stars and pointing the Kepler telescope to developing and running the photometric pipeline to curating and refining the catalogs of Kepler planets. We specifically thank Natalie Batalha, William Borucki, and David Ciardi in particular, for selecting stars in the Habitable Zone sample. EAP acknowledges support from Hubble Fellowship grant HST-HF2-51365.001-A awarded by the Space Telescope Science Institute, which is operated by the Association of Universities for Research in Astronomy,

Inc. for NASA under contract NAS 5-26555. AWH acknowledges NASA grant NNX12AJ23G. TDM acknowledges NASA grant NNX14AE11G. PAC acknowledges National Science Foundation grant AST-1109612. LH acknowledges National Science Foundation grant AST-1009810. LMW acknowledges support from Gloria and Ken Levy and from the Trottier Family. ES is supported by a post-graduate scholarship from the Natural Sciences and Engineering Research Council of Canada. IJMC performed his work under contract with the Jet Propulsion Laboratory (JPL) funded by NASA through the Sagan Fellowship Program executed by the NASA Exoplanet Science Institute. Work by JNW was partly supported by a NASA Keck PI Data Award, administered by the NASA Exoplanet Science Institute. This work made use of the SIMBAD database (operated at CDS, Strasbourg, France), NASA's Astrophysics Data System Bibliographic Services, and the NASA Exoplanet Archive, which is operated by the California Institute of Technology, under contract with the National Aeronautics and Space Administration under the Exoplanet Exploration Program. LAR gratefully acknowledges support provided by NASA through Hubble Fellowship grant #HF-51313 awarded by the Space Telescope Science Institute, which is operated by the Association of Universities for Research in Astronomy, Inc., for NASA, under contract NAS 5-26555. This work was performed in part under contract with the Jet Propulsion Laboratory (JPL) funded by NASA through the Sagan Fellowship Program executed by the NASA Exoplanet Science Institute. Finally, the authors wish to recognize and acknowledge the very significant cultural role and reverence that the summit of Maunakea has always had within the indigenous Hawaiian community. We are most fortunate to have the opportunity to conduct observations from this mountain.

REFERENCES

Adams, E. R., Ciardi, D. R., Dupree, A. K., Gautier, III, T. N., Kulesa, C., & McCarthy, D. 2012, AJ, 144, 42 Adams, E. R., Dupree, A. K., Kulesa, C., & McCarthy, D. 2013, AJ, 146, 9 Akeson, R. L., et al. 2013, PASP, 125, 989 Albrecht, S., et al. 2012, ApJ, 757, 18 Baranec, C., Ziegler, C., Law, N. M., Morton, T., Riddle, R., Atkinson, D., Schonhut, J., & Crepp, J. 2016, AJ, 152, 18 Barclay, T., et al. 2013, Nature, 494, 452 Bastien, F. A., Stassun, K. G., Basri, G., & Pepper, J. 2013, Nature, 500, 427 -. 2016, ApJ, 818, 43 Bastien, F. A., Stassun, K. G., & Pepper, J. 2014, ApJ, 788, L9 Batalha, N. M., et al. 2010a, ApJ, 713, L103 —. 2010b, ApJ, 713, L109 —. 2011, ApJ, 729, 27 –. 2013, ApJS, 204, 24 Borucki, W. J. 2016, Reports on Progress in Physics, 79, 036901 Borucki, W. J., et al. 2010, Science, 327, 977 —. 2011, ApJ, 736, 19 —. 2012, ApJ, 745, 120 -. 2013, Science, 340, 587 Brewer, J. M., Fischer, D. A., Basu, S., Valenti, J. A., & Piskunov, N. 2015, ApJ, 805, 126 Brewer, J. M., Fischer, D. A., Valenti, J. A., & Piskunov, N. 2016, ApJS, 225, 32 Brown, T. M., Latham, D. W., Everett, M. E., & Esquerdo, G. A. 2011, AJ, 142, 112 Bruntt, H., et al. 2010, MNRAS, 405, 1907 2012, MNRAS, 423, 122 Bryson, S. T., et al. 2010, ApJ, 713, L97

-. 2013, PASP, 125, 889

Buchhave, L. A., & Latham, D. W. 2015, ApJ, 808, 187 Buchhave, L. A., et al. 2012, Nature, 486, 375 -. 2014, Nature, 509, 593 Burke, C. J., et al. 2014, ApJS, 210, 19 2015, ApJ, 809, 8 Caldwell, D. A., et al. 2010, ApJ, 713, L92 Chiang, E., & Laughlin, G. 2013, MNRAS, 431, 3444 Christiansen, J. L., et al. 2012, PASP, 124, 1279 —. 2013, ApJS, 207, 35 —. 2015, ApJ, 810, 95 2016, ApJ, 828, 99 Chubak, C., Marcy, G., Fischer, D. A., Howard, A. W., Isaacson, H., Johnson, J. A., & Wright, J. T. 2012, arXiv:1207.6212 Coelho, P., Barbuy, B., Meléndez, J., Schiavon, R. P., & Castilho, B. V. 2005, A&A, 443, 735 Coughlin, J. L., et al. 2014, AJ, 147, 119 Cumming, A., Butler, R. P., Marcy, G. W., Vogt, S. S., Wright, J. T., & Fischer, D. A. 2008, PASP, 120, 531 Dawson, R. I., Murray-Clay, R. A., & Johnson, J. A. 2015, ApJ, De Cat, P., et al. 2015, ApJS, 220, 19 Désert, J.-M., et al. 2015, ApJ, 804, 59 Dong, S., et al. 2014, ApJ, 789, L3 Doyle, L. R., et al. 2011, Science, 333, 1602 Dressing, C. D., & Charbonneau, D. 2013, ApJ, 767, 95 -. 2015, ApJ, 807, 45 Endl, M., & Cochran, W. D. 2016, PASP, 128, 094502 Everett, M. E., Howell, S. B., Silva, D. R., & Szkody, P. 2013, ApJ, 771, 107 Fischer, D. A., & Valenti, J. 2005, ApJ, 622, 1102

Ford, E. B., et al. 2011, ApJS, 197, 2

Fressin, F., et al. 2013, ApJ, 766, 81

Furlan, E., et al. 2017, AJ, 153, 71 Gautier, III, T. N., et al. 2010, ArXiv e-prints . 2012, ApJ, 749, 15 Gilliland, R. L., et al. 2010, ApJ, 713, L160 $\,$. 2011, ApJS, 197, 6 Gómez Maqueo Chew, Y., et al. 2013, ApJ, 768, 79 Gustafsson, B., Edvardsson, B., Eriksson, K., Jørgensen, U. G., Nordlund, Å., & Plez, B. 2008, A&A, 486, 951 Haas, M. R., et al. 2010, ApJ, 713, L115 Hansen, B. M. S., & Murray, N. 2012, ApJ, 751, 158 Hebb, L., et al. 2009, ApJ, 693, 1920Heising, M. Z., Marcy, G. W., & Schlichting, H. E. 2015, ApJ, 814, 81 Hirano, T., Suto, Y., Winn, J. N., Taruya, A., Narita, N., Albrecht, S., & Sato, B. 2011, ApJ, 742, 69 Holczer, T., et al. 2015, ApJ, 807, 170 Howard, A. W., et al. 2010a, ApJ, 721, 1467 -. 2010b, Science, 330, 653 —. 2012, ApJS, 201, 15 -. 2013, Nature, 503, 381 Huber, D., et al. 2013, ApJ, 767, 127 -. 2014, ApJS, 211, 2 Isaacson, H., & Fischer, D. 2010, The Astrophysical Journal, 725, Jenkins, J. M., et al. 2010, in Society of Photo-Optical Instrumentation Engineers (SPIE) Conference Series, Vol. 7740 Jenkins, J. M., et al. 2015, AJ, 150, 56 Johnson, J. A., Aller, K. M., Howard, A. W., & Crepp, J. R. 2010, PASP, 122, 905 Kinemuchi, K., Barclay, T., Fanelli, M., Pepper, J., Still, M., & Howell, S. B. 2012, PASP, 124, 963 Kipping, D. M., Bakos, G. Á., Buchhave, L., Nesvorný, D., & Schmitt, A. 2012, ApJ, 750, 115 Koch, D. G., et al. 2010, ApJ, 713, L79 Kolbl, R., Marcy, G. W., Isaacson, H., & Howard, A. W. 2015, AJ, 149, 18 Kopparapu, R. K., et al. 2013, ApJ, 765, 131 Kruse, E., & Agol, E. 2014, Science, 344, 275 Kurucz, R. L. 1993, SYNTHE spectrum synthesis programs and line data Kurucz, R. L., Furenlid, I., Brault, J., & Testerman, L. 1984, Solar flux atlas from 296 to 1300 nm Kurucz, R. L., & Peytremann, E. 1975, SAO Special Report, 362 Lissauer, J. J., et al. 2011a, Nature, 470, 53 —. 2011b, ApJS, 197, 8 —. 2012, ApJ, 750, 112

-. 2014, ApJ, 784, 44

Marcy, G. W., & Butler, R. P. 1992, PASP, 104, 270

Marcy, G. W., et al. 2014, ApJS, 210, 20

Mathur, S., et al. 2016, ArXiv e-prints

Mayor, M., et al. 2011, arXiv:1109.2497

Morton, T. D. 2012, ApJ, 761, 6

McCauliff, S. D., et al. 2015, ApJ, 806, 6

15, 1095

N. M. 2016, ApJ, 822, 86 Morton, T. D., & Johnson, J. A. 2011, ApJ, 738, 170 Moutou, C., et al. 2013, A&A, 558, L6 Mullally, F., et al. 2015, ApJS, 217, 31 Pál, A., et al. 2008, ApJ, 680, 1450 Pepe, F., et al. 2013, Nature, 503, 377 Petigura, E. A. 2015, PhD thesis, University of California, Berkeley Petigura, E. A., Howard, A. W., & Marcy, G. W. 2013a, Proceedings of the National Academy of Science, 110, 19273 Petigura, E. A., Marcy, G. W., & Howard, A. W. 2013b, ApJ, 770, 69 Pinsonneault, M. H., An, D., Molenda-Żakowicz, J., Chaplin, W. J., Metcalfe, T. S., & Bruntt, H. 2012, ApJS, 199, 30 Piskunov, N. E. 1992, in Physics and Evolution of Stars: Stellar Magnetism, ed. Y. V. Glagolevskij & I. I. Romanyuk, 92 Quintana, E. V., et al. 2014, Science, 344, 277 Rogers, L. A. 2015, ApJ, 801, 41 Rowe, J. F., et al. 2014, ApJ, 784, 45 . 2015, ApJS, 217, 16 Sanchis-Ojeda, R., Rappaport, S., Winn, J. N., Kotson, M. C., Levine, A., & El Mellah, I. 2014, ApJ, 787, 47 Santerne, A., et al. 2012, A&A, 545, A76 Seager, S. 2013, Science, 340, 577 Smith, J. C., Morris, R. L., Jenkins, J. M., Bryson, S. T., Caldwell, D. A., & Girouard, F. R. 2016, PASP, 128, 124501 Smith, J. C., et al. 2012, PASP, 124, 1000 Sneden, C. A. 1973, PhD thesis, The University of Texas at Austin. Stempels, H. C., Collier Cameron, A., Hebb, L., Smalley, B., & Frandsen, S. 2007, MNRAS, 379, 773 Stumpe, M. C., et al. 2012, PASP, 124, 985 Tenenbaum, P., et al. 2013, ApJS, 206, 5 2014, ApJS, 211, 6 Thompson, S. E., Mullally, F., Coughlin, J., Christiansen, J. L., Henze, C. E., Haas, M. R., & Burke, C. J. 2015, ApJ, 812, 46 Torres, G., Andersen, J., & Giménez, A. 2010, A&A Rev., 18, 67 Torres, G., Fischer, D. A., Sozzetti, A., Buchhave, L. A., Winn, J. N., Holman, M. J., & Carter, J. A. 2012, ApJ, 757, 161 Torres, G., et al. 2011, ApJ, 727, 24 2015, ApJ, 800, 99 Twicken, J. D., et al. 2016, AJ, 152, 158 Valenti, J. A., & Fischer, D. A. 2005, ApJS, 159, 141 Valenti, J. A., & Piskunov, N. 1996, A&AS, 118, 595 Verner, G. A., et al. 2011a, MNRAS, 415, 3539 Luo, A.-L., et al. 2015, Research in Astronomy and Astrophysics, 2011b, ApJ, 738, L28 Vogt, S. S., et al. 1994, in Proc. SPIE Instrumentation in Astronomy VIII, David L. Crawford; Eric R. Craine; Eds., Vol. 2198, p. 362 Weiss, L. M., & Marcy, G. W. 2014, ApJ, 783, L6 Wolfgang, A., & Lopez, E. 2015, ApJ, 806, 183 Wu, Y., Du, B., Luo, A., Zhao, Y., & Yuan, H. 2014, in IAU Symposium, Vol. 306, Statistical Challenges in 21st Century Cosmology, ed. A. Heavens, J.-L. Starck, & A. Krone-Martins, Ziegler, C., et al. 2017, AJ, 153, 66

Morton, T. D., Bryson, S. T., Coughlin, J. L., Rowe, J. F.,

Ravichandran, G., Petigura, E. A., Haas, M. R., & Batalha,